Ore Geology Reviews 87 (2017) 100–113

Contents lists available at ScienceDirect

Ore Geology Reviews

journal homepage: www.elsevier.com/locate/oregeorev

Controls on the distribution of rare earth elements in deep-sea sediments in the North Atlantic Ocean

Amaya Menendez [a,*], Rachael H. James [a], Stephen Roberts [a], Kate Peel [b], Douglas Connelly [b]

[a] Ocean and Earth Science, National Oceanography Centre Southampton, University of Southampton Waterfront Campus, European Way, Southampton SO14 3ZH, UK
[b] National Oceanography Centre, Waterfront Campus, University of Southampton, Southampton SO14 3ZH, UK

ARTICLE INFO

Article history:
Received 8 April 2016
Received in revised form 9 September 2016
Accepted 15 September 2016
Available online 1 October 2016

Keywords:
Rare earth elements
Fe-Mn micronodules
Atlantic deep sediments
Seafloor mining
Fe-Mn-(oxyhydr)oxides

ABSTRACT

Deep-sea sediments can contain relatively high concentrations of rare earth elements and yttrium (REY), with a growing interest in their exploitation as an alternative to land-based REY resources. To understand the processes that lead to enrichment of the REY in deep-sea sediments, we have undertaken a detailed geochemical study of sediments recovered from the Atlantic Ocean, on a transect along ~24°N that includes the deep Nares Abyssal Plain and the Canary and North America Basins.

Total REY concentrations (ΣREY) range from 7.99 to 513 ppm, and total concentrations of the heavy REY (Eu - Lu) range from 0.993 to 56.3 ppm. REY concentrations are highest in slowly accumulating pelagic red clays, especially in samples that contain ferromanganese micronodules. Factor analysis reveals that hydrogenous Fe- and Mn-(oxyhydr)oxides are the primary REY carrier phase in the red clays. In situ analysis of individual micronodules confirms that they have high ΣREY (up to 3620 ppm). REY concentrations are higher in micronodules that have a hydrogenous source, characterised by higher Fe/Mn, compared to micronodules that have a diagenetic source.

The ΣREY content of North Atlantic deep-sea sediments is ~4 times lower than in Pacific deep-sea sediments. We calculate that the area of seafloor required to extract ~10% of the global annual REY demand is ~100 km^2, assuming removal of the upper 1 m of sediment.

1. Introduction

The rare earth elements (REE) are a group of 17 chemically similar metallic elements which comprise the 15 lanthanides, as well as scandium and yttrium. They are used in the widest range of consumer products of any group of elements, and are important in many 'green' carbon-reducing technologies (Castor and Hedrick, 2006). For example, wind turbines use in the range of 0.6–1.0 t of neodymium magnets per megawatt of energy generated, REE phosphors are used in energy efficient lighting including LEDs, and 10–15 kg of lanthanum is used in every rechargeable battery that powers the Toyota Prius hybrid car (Lifton, 2009).

The world's most commercially important REE deposits are found in alkaline igneous rocks and carbonatites (Orris and Grauch, 2002). The estimated total world reserve of rare earth oxides on land is about 114 million tonnes, 48% of which is in China (Cordier, 2011). World production of REE is currently dominated by China, accounting for 90% of supply in 2013 (USGS, 2014). Demand for the REE is expected to grow by at least 6% per year over the next 25 years, particularly for permanent magnets and medical technologies (Alonso et al., 2012), and this, coupled with China's near monopoly of production, has led to concern about the risk of supply shortage, and prompted increased interest in REE exploration and the emergence of small land-based mines in other parts of the world (Australia, South Africa, North and South America and Scandinavia; Orris and Grauch, 2002).

Potential marine-based REE resources include deep sea sediments, polymetallic nodules, ferromanganese crusts and phosphorites. Polymetallic nodules mainly occur in deep ocean basins at depths of 4000–6000 m (Zhang et al., 2012). They have very high total REE concentrations (~700–2400 ppm; Hein and Koschinsky, 2013) as well as high concentrations of other economically interesting metals such as Ni, Co, Cu, Mo, Li and Te (Hein et al., 2013). The nodules can acquire REEs and metals from seawater ("hydrogenous" nodules) or from the sediment pore waters ("diagenetic" nodules) (Halbach et al., 1981). Ferromanganese crusts form by precipitation of dissolved components from seawater and are commonly found on top of western Pacific guyots. They are mainly formed of Mn-oxides intergrown with Fe oxyhydroxides; some older (pre-middle Miocene) crusts also contain carbonate fluoroapatite that was incorporated during diagenesis (Hein et al., 1993). The crusts have unusually high concentrations of Co (~8000 ppm; e.g. Koschinsky and Hein, 2003), and total REE

* Corresponding author.
E-mail address: A.Menendez@soton.ac.uk (A. Menendez).

http://dx.doi.org/10.1016/j.oregeorev.2016.09.036
0169-1368/

concentrations (~2000 ppm; e.g. Mills et al., 2001) that are similar to polymetallic nodules. Phosphorite deposits are widespread on the seafloor of continental shelves and slopes along the western continental margins of the Pacific and Atlantic oceans, and can also occur on seamounts and plateaus (e.g. Thomson et al., 1984). Like ferromanganese crusts, they acquire REEs from seawater, but their total REE concentration is widely variable (from a few tens to ~2000 ppm; Gonzalez et al., 2016).

Deep-sea sediments, including pelagic red clay, metalliferous sediments and zeolitic clay, are a potential source of REE. High concentrations of the REE and yttrium (REY), up to 2230 ppm total REY (ΣREY), comparable to the level in ore deposits in southern China, are reported for deep sea muds in the eastern South Pacific and central North Pacific (Kato et al., 2011). These authors suggest that the 70-m thick REY-rich mud layer in an area of 1 km^2 in the central North Pacific could supply the majority of current annual REY consumption in the world. If REY levels in Pacific sediments are applicable throughout the world's oceans, then the seafloor REY resource could potentially exceed the world's current land reserves (Kato et al., 2011).

To assess the potential for deep-sea sediments from the Atlantic Ocean as a REY resource, we have measured REY concentrations in sediments recovered from a transect at ~24°N (Fig. 1). We also use these data to evaluate the processes that lead to REE enrichment. We show that ΣREY concentrations are lower than those measured in the eastern South Pacific and central North Pacific, and highlight the roles of scavenging of REY by iron- and manganese oxy(hydr)oxides and micronodule formation for enhancing REY concentrations in deep sea sediments.

2. Sample material

Sediment samples (~8 cm^3) were collected from cores stored at the British Ocean Sediment Core Facility, Southampton (BOSCORF) and at the Lamont-Doherty Earth Observatory, New York (LDEO). The cores were collected between 1955 and 1988 on cruises Discovery 118 (1981) and 177 (1988), Atlantis 180 and 181 (1947), Conrad 10 (1965), 11 (1968) and 21 (1978), Theta 1 (1971), Kane 74 (1974), Kevin Moran 1 (1955) and Vema 9 (1956), 10 (1956), 16 (1959), 17 (1960), 20 (1964), 22 (1966), 23 (1966), 25 (1968), 27 (1970), 29 (1973), 30 (1973) and 32 (1975). Most of these cores were split on board the ship or shortly after they were collected, and have since been stored at room temperature, in the case of the LDEO cores, and at ~4 °C in the case of the cores at BOSCORF. Core RC21-02 had been stored refrigerated at ~4 °C and was split for sampling in this study. The old age and partly desiccated state of some of the cores raises the possibility of chemical alteration during storage, although this effect is considered to be minor in oxic sediments (Rapin et al., 1986).

The core sites are located on a transect at ~24°N across the North Atlantic Ocean, east to west from the Great Bahama Bank to the west slope of Africa. The transect crosses through the Nares Abyssal Plain, the North America Basin and the Canary Basin, and intersects the Snake Pit hydrothermal site at ~23°N. The location of the core sites is showed in Fig. 1, and a list of the samples including water depth and a brief description is given in Table 1.

The sediment samples include fine-grained red/brown clays, grey clays, turbidites, carbonate oozes, chalks of different purities and foraminiferal marls. The red/brown clays are quite compacted and tend to be continuous in the cores, although traces of burrowing were observed in some cores. Core lithology was logged using a hand lens to assess texture and colour, structures such as bedding and burrows, carbonate content, mineralogy and the nature of the contact between different intervals. Samples were selected from the best preserved sections, and on the basis of the lithology.

Photographs of representative cores are shown in Fig. 2. Some sediments host palagonitised volcanic glass fragments and micronodules, within a fine-grained clay matrix (Fig. 3). The micronodules are ~0.1 to 5 mm in diameter, are rounded or subrounded and are generally evenly distributed throughout the sediment. Micronodules in sample VM25-033 (Fig. 3c) exhibit a dendritic morphology, and are observed to cover large zeolite/palagonite clasts. The micronodules are numerous in some sediment samples, comprising up to 5% of the matrix.

3. Analytical methods

3.1. Sample dissolution

Sediment samples were taken from the inner part of the recovered cores to avoid the sampling of surface alteration products. The samples were then oven-dried at 40 °C (a low temperature was used to minimise the likelihood for modification of Fe concentrations in these oxic

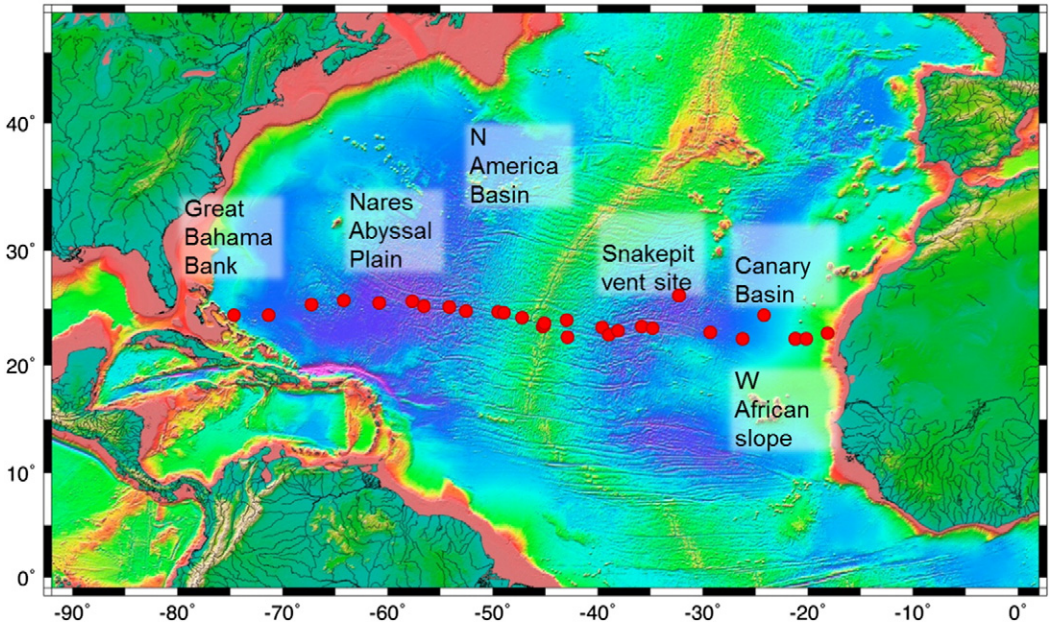

Fig. 1. Location of sediment samples used in this study. The samples were taken along a transect across the North Atlantic at ~24°N. Seafloor topography is from NOAA (http://oceanexplorer.noaa.gov/explorations/05stepstones/background/plan/media/natl_topography.html).

Table 1
Location and description of deep-sea sediments from the North Atlantic Ocean.

Sample	Lat (°N)	Long (°W)	Location	Water depth (m)	Core type[#]	Source[*]	Depth bsf (cm)	Description
RC10-277	24.0	72.9	Great Bahama Bank	5407	PC	LDEO	4–6	Carbonate sand
RC11-243	24.0	69.6	Great Bahama Bank	5407	PC	LDEO	30–32	Brown clay
VM17-2	24.9	65.5	Great Bahama Bank	5303	PC	LDEO	200–202	Consolidated brown clay
VM16-15	25.3	62.5	Nares Abyssal Plain	5810	PC	LDEO	880–882	Consolidated brown clay
VM09-34	25.1	59.2	Nares Abyssal Plain	5879	TC	LDEO	500–502	Consolidated brown clay
RC10-10	25.2	56.1	Nares Abyssal Plain	5929	PC	LDEO	500–502	Consolidated brown clay
RC10-13	24.8	55.0	Nares Abyssal Plain	5300	PC	LDEO	85–87	Brown-yellowish clay
VM25-33	24.7	52.6	North America Basin	941	PC	LDEO	40–42	Orange-brown clay with micronodules
VM25-32	24.4	51.0	North America Basin	5464	PC	LDEO	100–102	Brown clay with micronodules
VM25-30	24.3	48.0	W of Mid-Atlantic Ridge	4096	PC	LDEO		Chalk
VM10-93	24.2	47.5	Central Atlantic	3574	PC	LDEO	100–102	Carbonate ooze
VM31-152	23.8	45.8	Central Atlantic	4174	PC	LDEO	200–202	Marl
VM10-89	23.0	43.8	Central Atlantic	3523	PC	LDEO	630–632	White chalk
TH1-54S	23.1	43.8	Central Atlantic	3840	CMC	LDEO	50–52	Consolidated pink clay
VM20-242	23.4	43.7	Central Atlantic	4565	PC	LDEO	635–637	Carbonate-rich brown clay with micronodules
AT180-118	23.6	41.6	Central Atlantic	4500	PC	LDEO	200–202	Grey silty clay
VM20-241	22.1	41.5	Central Atlantic	4372	PC	LDEO	100–102	Foraminiferous marl
VM10-88	23.0	38.2	Central Atlantic	4971	PC	LDEO	400–402	Consolidated brown clay
AT181-001	22.3	37.6	Central Atlantic	3895	PC	LDEO	65–67	Chalk
RC21-2	22.7	36.7	Canary Basin	3895	PC	LDEO	20–22	Red-brown clay
VM22-212	23.0	34.5	Canary Basin	6081	PC	LDEO	750–752	Brown clay with micronodules
VM10-87	22.9	33.5	Canary Basin	5329	PC	LDEO	420–422	Consolidated grey clay
D11805-7	25.7	31.0	Canary Basin	6129	BC	BOSCORF	15–17, 38–40	Turbiditic grey clay
D10311	25.7	31.0	Canary Basin	6133	GC	BOSCORF	5–7, 40–42	Red clay
D11805-5	25.7	31.0	W Africa cont. slope	5554	PC	BOSCORF	59–71, 96–98	Turbiditic grey clay
VM27-255	22.6	28.0	W Africa cont. slope	5554	PC	LDEO	81–83	Orange clay
VM32-52	22.0	25.0	W Africa cont. slope	5220	PC	LDEO	38–40	Marl
KA74-4	24.0	23.0	W Africa cont. slope	4838	GC	LDEO	323–325	Consolidated brown clay
VM23-99	22.0	20.0	W Africa cont. slope	4118	PC	LDEO	85–87	Yellow marl
VM29-170	22.0	20.0	W Africa cont. slope	4455	PC	LDEO	7–9	Marl
VM30-54	22.0	19.0	W Africa cont. slope	3506	PC	LDEO	140–142	Marl
KM1-46	22.5	17.0	W Africa cont. slope	1221	PC	LDEO	50–52	Grey sand

[#] PC = piston core; GC = gravity core; BC = box core; KC = Kasten core; CMC = camera-mounted core; TC = trigger core; RD = rock dredge.
[*] LDEO = Lamont-Doherty Earth Observatory; BOSCORF = British Ocean Sediment Core Facility. bsf = below seafloor.

sediments; Rapin et al., 1986) and ground in an agate mortar and dissolved in a mixture of hydrofluoric (HF), perchloric ($HClO_4$) and hydrochloric (HCl) acids, and aqua regia. For each sample, ~100 mg of powdered material was transferred to a 15 mL PTFE screw-cap vial and weighed. 5 mL of aqua regia was added to each vial, which was capped and refluxed on a hotplate at 90 °C overnight. The solution was then evaporated to near dryness, and 3 mL of HF and 2.25 mL of $HClO_4$ were added and heated on a hotplate at 150 °C overnight. The cap was removed and the samples were heated to 170 °C until white fumes were observed. The temperature was then increased to 180 °C and the sample was evaporated to near-dryness. 2 mL of $HClO_4$ was added, the cap was replaced and the solution was heated overnight on a hotplate at 150 °C. After evaporating to near-dryness, 10 mL of HCl was added and the sample was heated on a hotplate at 130 °C.

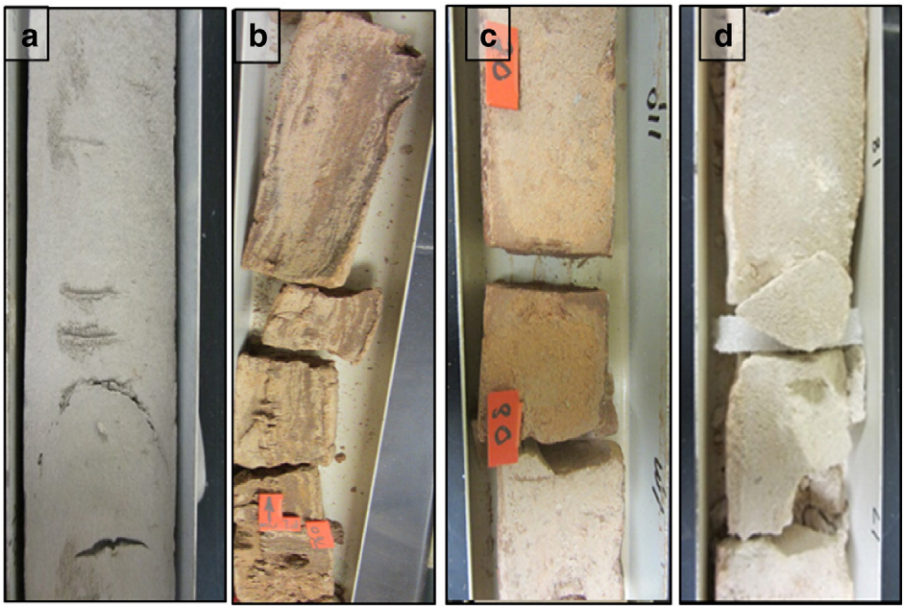

Fig. 2. Representative sediment cores of a) grey clay (VM10-87), b) micronodule-rich red/brown clay (VM22-212), c) red/brown clay (VM27-255) and d) carbonate ooze (AT181-1).

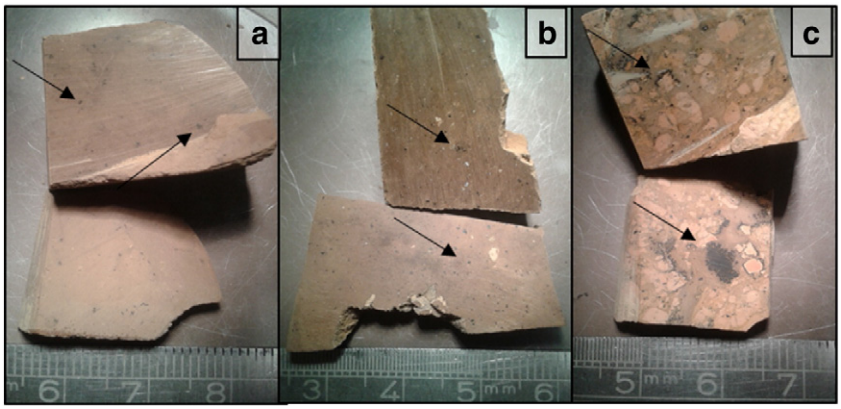

Fig. 3. Micronodules in samples a) VM25-032, b) VM20-242 and c) VM25-033.

The solution was then evaporated to near dryness, and made up to 100 cm^3 in 0.5 M HNO_3 in a volumetric flask. A sub-sample of 1 mL of this solution was dried down, spiked with an internal standard consisting of 5 ppm Re and In and 20 ppm Be, and made up to 13 mL with 0.5 M HNO_3 for trace element and REY analyses. For analysis of the major elements, 0.25 mL of the solution was spiked, and made up to 5 mL with 0.5 M HNO_3.

3.2. Analysis of major elements, trace elements and REYs

Major element (Na, Mg, Al, K, Ca, Ti, Fe and Mn), trace element (V, Cr, Co, Ni, Cu, Zn, Rb, Sr and Ba), and REY (La, Ce, Pr, Nd, Sm, Eu, Gd, Tb, Dy, Y, Ho, Er, Tm and Lu) concentrations were determined by inductively coupled plasma mass spectrometry (ICP-MS; Thermo Scientific X-Series II) at the University of Southampton. Measurements were calibrated against 6 certified rock reference materials (BHVO-2, BAS-206, BIR-1, JB-1a, BRR-1, JB-3), and the accuracy and reproducibility of the measurements was assessed by multiple (n = 9) analyses of MAG-1, BCSS-1 and MESS-1 certified reference materials, analysed as unknowns alongside the samples. Instrument drift was assessed by addition of internal standards (Re, In and Be), and analysis of an internal standard every 10 samples. The external reproducibility of the analyses was better than ±5% for the major elements, and better than ±3% for most of the trace elements and REEs; the reproducibility of Cu and Y analyses was ±8% and ±15%, respectively. Measured concentrations were within ±5% of the certified or recommended values for all elements except K (±10%), Tb (±20%) and Y (±15%).

Table 2
Concentrations (wt%) of major elements in North Atlantic deep-sea sediments. Bdl = below detection limit.

Sample	Type[a]	Depth (m)	Na	Mg	Al	K	Ca	Ti	Fe	Mn	$CaCO_3$
RC10-277	Carb	5407	2.94	1.89	2.41	1.11	28.5	0.17	2.75	0.33	58.8
RC11-243	RC	5407	1.80	1.52	6.76	2.48	5.24	0.36	4.23	0.14	12.6
VM17-002	RC	5303	2.14	1.39	8.46	2.37	0.32	0.37	5.35	0.54	bdl
VM16-015	RC	5809	0.86	1.67	10.7	2.91	0.31	0.48	6.44	0.47	bdl
VM9-34	RC	5879	1.83	1.67	10.2	3.12	0.47	0.49	7.05	0.33	bdl
RC10-10	RC	5929	1.29	1.35	9.60	2.60	0.29	0.44	6.19	0.46	bdl
RC10-13	RC	5300	1.78	1.61	9.29	2.63	3.99	0.46	5.91	0.58	7.4
VM25-33	RC†	5009	1.82	2.72	8.80	2.50	0.65	0.44	7.65	0.69	bdl
VM25-32	RC†	5464	1.37	1.84	9.38	2.86	0.69	0.50	6.46	0.62	0.1
VM25-30	Carb	4096	1.88	0.76	3.07	1.05	29.0	0.18	2.31	0.21	64.3
VM10-093	Carb	3574	2.83	0.24	0.58	0.25	40.9	0.03	0.52	0.07	90.4
VM31-152	Carb	4174	3.25	0.21	0.29	0.14	28.5	0.02	0.33	0.05	93.0
VM10-89	Carb	3523	1.44	0.35	0.95	0.32	36.9	0.06	0.78	0.07	82.7
TH1-54S	Carb	3840	0.83	0.72	2.49	0.81	30.7	0.15	1.87	0.15	65.2
VM20-242	RC†	4565	0.81	2.57	7.98	2.03	6.90	0.47	7.49	1.04	11.7
AT180-118P	GC	4500	0.84	1.40	8.33	2.59	2.17	0.56	4.86	0.44	3.4
VM20-241	Carb	4372	1.16	0.59	3.15	0.92	29.4	0.20	2.55	0.90	68.4
VM10-88	RC†	4971	1.51	1.62	10.0	2.37	0.62	0.64	8.79	0.75	bdl
AT181-1	Carb	3895	1.61	2.68	0.09	0.06	39.5	0.001	0.14	0.003	94.3
RC21-02	RC	3895	1.23	1.42	8.36	2.41	4.57	0.52	5.12	0.10	9.2
VM22-212	RC†	6081	1.43	2.81	7.80	3.09	0.57	0.40	8.87	0.64	9.2
VM10-87	GC	5329	0.89	1.26	9.73	3.15	0.79	0.52	4.81	0.45	bdl
D11805_7-S1	GC	6129	2.38	1.22	4.83	1.47	21.2	0.26	2.83	0.41	0.1
D11805_7-S2	GC	6129	1.97	1.22	4.78	1.48	20.9	0.26	2.79	0.41	42.3
D10311-S1	RC	6133	1.70	2.06	9.28	2.75	0.91	0.58	5.93	0.28	46.9
D10311-S2	RC	6133	1.65	1.89	8.88	2.65	1.16	0.55	5.84	0.34	0.2
D11805_5-S1	GC	5554	1.69	1.20	4.64	1.44	20.4	0.25	2.73	0.39	0.9
D11805_5-S2	GC	5554	2.11	1.26	4.75	1.47	20.9	0.25	2.84	0.40	46.4
VM27-255	RC	5554	2.35	1.85	9.21	2.70	1.11	0.56	6.16	0.44	40.0
VM32-52	Carb	5220	1.73	1.84	8.59	2.58	3.02	0.53	5.41	0.19	90.6
KA74-0046	RC	4838	1.89	1.31	6.11	1.82	14.9	0.41	3.88	0.13	5.5
VM23-99	Carb	4118	2.33	1.18	3.90	1.28	21.7	0.22	1.97	0.07	31.3
VM29-170	Carb	4455	2.03	0.71	2.59	0.81	32.3	0.19	1.65	0.04	45.4
VM30-54	Carb	3506	1.34	0.84	2.56	0.97	25.1	0.15	1.42	0.02	71.8
KM1-046P	GC	1221	1.75	0.81	2.19	0.90	25.5	0.14	1.23	0.009	57.5

[a] Carb = carbonate; RC = red clay; RC† = red clay with micronodules; GC = grey clay.

Table 3
Concentrations (ppm) of minor elements in North Atlantic deep-sea sediments.

Sample	Type[a]	Depth (m)	V	Cr	Co	Ni	Cu	Rb	Sr	Ba
RC10-277	Carb	5407	49.9	39.5	41.5	80.1	65.4	26.3	421	101
RC11-243	RC	5407	103	75.0	18.9	42.4	42.5	108	285	336
VM17-002	RC	5303	151	67.5	57.7	102	85.3	112	88.1	332
VM16-015	RC	5809	193	83.7	55.0	89.9	86.6	141	115	401
VM9-34	RC	5879	164	85.2	46.0	79.8	97.3	142	134	454
RC10-10	RC	5929	151	81.2	61.4	107	124	127	109	361
RC10-13	RC	5300	149	84.5	70.4	150	134	124	283	362
VM25-33	RC†	5009	133	74.1	64.3	466	185	98.1	113	171
VM25-32	RC†	5464	161	82.2	80.5	136	148	123	152	374
VM25-30	Carb	4096	57.8	33.8	28.8	48.4	58.9	40.8	1230	346
VM10-093	Carb	3574	14.0	8.38	8.14	12.8	21.2	7.52	1600	49.2
VM31-152	Carb	4174	7.84	4.64	5.62	9.49	12.4	3.43	935	14.8
VM10-89	Carb	3523	21.0	10.5	10.3	16.4	26.8	11.8	1420	84.2
TH1-54S	Carb	3840	46.9	28.2	21.2	32.6	45.3	31.3	1360	280
VM20-242	RC†	4565	268	66.7	131	185	205	84.8	408	343
AT180-118P	GC	4500	119	63.8	12.7	23.2	16.5	122	188	315
VM20-241	Carb	4372	54.6	33.2	16.5	30.7	44.8	36.5	1110	143
VM10-88	RC†	4971	207	53.7	76.3	178	184	89.8	159	271
AT181-1	Carb	3895	1.41	14.9	0.26	4.71	12.6	0.097	2990	9.83
RC21-02	RC	3895	123	60.2	15.3	30.2	39.5	115	284	474
VM22-212	RC†	6081	244	89.2	73.4	209	152	99.9	137	320
VM10-87	GC	5329	117	90.9	14.0	35.3	24.5	146	117	457
D11805_7-S1	GC	6129	73.1	71.4	9.48	36.9	44.0	56.9	991	485
D11805_7-S2	GC	6129	74.0	71.0	9.40	38.5	44.6	58.5	1000	488
D10311-S1	RC	6133	137	101	39.8	110	87.1	108	145	357
D10311-S2	RC	6133	141	90.6	51.4	106	124	110	167	347
D11805_5-S1	GC	5554	70.2	70.2	9.79	38.9	45.8	57.9	983	483
D11805_5-S2	GC	5554	73.7	73.1	9.59	38.0	45.0	56.7	988	480
VM27-255	RC	5554	131	95.0	15.3	55.9	92.4	113	149	380
VM32-52	Carb	5220	125	88.5	28.3	76.5	107	105	222	433
KA74-0046	RC	4838	88.0	71.6	18.7	47.5	72.1	72.7	735	366
VM23-99	Carb	4118	58.3	71.4	7.08	37.6	62.2	47.2	936	842
VM29-170	Carb	4455	41.9	27.5	6.50	17.0	35.8	28.3	1400	230
VM30-54	Carb	3506	41.7	36.1	5.34	28.7	28.0	33.1	1090	490
KM1-046P	GC	1221	30.4	36.6	2.71	18.7	10.6	27.9	947	233

[a] Carb = carbonate; RC = red clay; RC† = red clay with micronodules; GC = grey clay.

3.3. $CaCO_3$ analysis

Total inorganic carbon was measured by separating CO_2 from 15 mg of sediment by addition of 0.4 M phosphoric acid (H_3PO_4), and analysis of the CO_2 produced by coulometry (UIC Inc. CM5015 CO_2 coulometer, equipped with an acidification module). A 99.999% purity $CaCO_3$ standard was used to calibrate the measurements, and to assess drift and reproducibility. The reproducibility of the analyses is better than ±0.5%.

3.4. Laser ablation ICP-MS analyses of micronodules

Thick sections were made of consolidated sediments containing micronodules, and these were mounted onto a glass sample holder along with polished chips of NIST 610 and NIST 612 glass standard reference materials. Fig. 3 shows the distribution of micronodules in some of these thick sections.

Laser ablation ICP-MS analyses of these materials were conducted at the University of Southampton using a 193 nm excimer laser (New Wave Research model UP193X) coupled to a quadrupole ICP-MS (Thermo X-Series II). Element concentrations were determined on 50 μm diameter spots on each nodule. Ablations were conducted with a laser power of ~75% and a repetition rate of 5 Hz, in a He atmosphere. For each analysis, the gas blank was measured first with the laser beam blocked by a shutter. The shutter was then removed, and the transient signals from the analyte were collected for the ablation period. Data was acquired for Mn, Fe, Cu, Ti, V, Co, Ni, Ba, U, Th and the REYs. Raw counts were processed off line using standard spreadsheet software, and measurements were calibrated using the NIST 612 and NIST 610 glass standards. The reproducibility of the analyses (assessed by multiple (n = 30) measurements of the NIST-612 standard) was better than ±5% for all elements except Cu (±17%) and V (±13%). The accuracy of the analyses (assessed by measuring NIST-610 as an unknown) was better than ±5% for all elements except Sm and Ho (better than ±10%).

4. Results

Concentrations of major, minor and REY elements in the sediment samples are given, respectively, in Tables 2, 3 and 4. Results of laser ablation analyses of metal and REY concentrations in 3 representative micronodules from each of the micronodule-containing samples (VM10-88, VM20-242, VM25-033, VM25-032 and VM22-212) are given in Tables 5 and 6. A total of 14 micronodules were analysed from sample VM10-88, 49 from VM20-242, 86 from VM25-033, 19 from VM25-032 and 49 from VM22-212.

4.1. Chemical composition of North Atlantic deep-sea sediments

The red and grey clays are characterised by relatively high concentrations of elements associated with detrital material, including Ti (0.14–0.64 wt%), Mg (0.81–2.06 wt%), Al (2.19–10.7 wt%), K (0.90–3.15 wt%), Rb (27.9–146 ppm), and Fe (1.23–7.05 wt%), whereas carbonate sediments have relatively high concentrations of Ca (3.02–40.9 wt%) and Sr (222–2990 ppm). The $CaCO_3$ content of the sediments generally decreases with increasing water depth, but is relatively lower close to the continental shelf (~31 to 72 wt%).

The red clays have the highest Fe concentrations (3.88–7.05 wt%), and the micronodule-rich red clays are notably Fe- (6.46–8.87 wt%) and Mn- (0.62–1.04 wt%) rich compared to the other red clay samples. The red clays also have the highest concentrations of V (88.0–268 ppm), Cr (53.7–101 ppm), Co (12.7–131 ppm), Ni (30.2–466 ppm) and Cu (39.5–205 ppm); the micronodule-rich red clays have higher V (133–268 ppm), Co (64.3–131 ppm), Ni (136–466 ppm) and Cu (148–205 ppm) (but not Cr (53.7–89.2 ppm)) compared to the red clays that do not contain micronodules.

Similarly, ΣREY concentrations are highest in the red clays and lower in the grey clays that contain significant terrigenous material transported by turbidites (Thomson et al., 1984), and lowest in carbonate ooze. ΣREY concentrations in the red clays (Table 4) vary from 194 to 513 ppm, and the average value is 310 ppm. Highest ΣREY concentrations are found in the red clay samples that contain micronodules (up to 513 ppm). The total HREE (Eu, Gd, Tb, Dy, Ho, Er, Tm, Yb and Lu) content of the red clays is 18–55 ppm. For the grey clays, ΣREY concentrations vary between 66 to ~262 ppm (average 145 ppm), and HREE concentrations are 13–23 ppm. Carbonate-rich sediments have ΣREY concentrations of between 7.8 and 267 ppm (average 120 ppm) and HREE concentrations vary from ~7 to 30 ppm.

Red clays containing micronodules that were observable in hand specimen are variably enriched or depleted in Ce relative to La and Nd. There is a positive Ce anomaly in sample VM25-32 (1.48) but the Ce anomaly is slightly negative (0.82–0.96) in the rest of the micronodule-containing samples. All the red clay samples without micronodules have positive Ce anomalies (1.03 to 1.52), whereas Ce is variably enriched or depleted relative to La and Nd in the grey clays ($Ce^* = 0.91$ to 1.13). Most of the carbonate-rich samples have negative Ce anomalies, as low as 0.53. However samples RC10-277 and VM32-52, which are located close to the continental slope, have positive Ce anomalies. LREE/HREE ratios indicate that grey and red clays, including the micronodule-rich red clays, are enriched in the LREE relative to the HREE, whereas most of the carbonates are enriched in the HREE relative to the LREE.

4.2. Chemical composition of micronodules

Micronodules that were observable in hand specimen were found in samples VM20-242, VM10-088 (Central Atlantic), VM25-32, VM25-33

Table 4
Concentrations (ppm) of rare earth elements and yttrium (REY) in North Atlantic deep-sea sediments.

Sample	Type[a]	Depth (m)	La	Ce	Pr	Nd	Sm	Eu	Gd	Tb	Dy	Y	Ho	Er	Tm	Yb	Lu	ΣREY	LREE/HREE	Ce*
RC10-277	Carb	5407	8.97	42.2	2.22	8.74	1.90	0.47	1.97	0.31	1.82	11.0	0.37	1.06	0.16	1.03	0.16	82.5	0.77	2.36
RC11-243	RC	5407	39.1	86.9	9.63	35.7	6.75	1.36	5.67	0.85	4.80	26.4	0.94	2.59	0.38	2.43	0.36	224	1.38	1.15
VM17-002	RC	5303	48.9	128	12.4	46.3	9.40	2.04	8.32	1.24	6.94	36.8	1.34	3.62	0.52	3.36	0.50	310	1.27	1.33
VM16-015	RC	5809	44.3	115	11.0	40.4	7.99	1.69	6.71	1.01	5.70	29.0	1.10	3.01	0.44	2.84	0.42	270	1.34	1.34
VM9-34	RC	5879	46.0	122	11.4	41.9	8.07	1.66	6.55	0.99	5.60	28.1	1.08	2.98	0.44	2.91	0.43	280	1.38	1.38
RC10-10	RC	5929	48.2	140	11.9	43.7	8.62	1.79	7.12	1.09	6.18	31.0	1.19	3.30	0.48	3.16	0.48	308	1.31	1.52
RC10-13	RC	5300	47.4	129	12.0	43.4	8.60	1.80	7.30	1.09	6.21	33.7	1.20	3.31	0.48	3.10	0.46	298	1.31	1.41
VM25-33	RC†	5009	59.6	101	16.0	62.2	13.4	3.03	12.3	1.87	10.7	58.7	2.08	5.59	0.78	4.89	0.71	352	1.11	0.82
VM25-32	RC†	5464	53.8	156	13.6	51.0	10.3	2.20	8.91	1.34	7.54	39.7	1.45	3.94	0.57	3.67	0.55	355	1.28	1.48
VM25-30	Carb	4096	32.0	61.1	8.53	33.0	6.78	1.46	6.19	0.91	5.10	28.7	0.97	2.58	0.36	2.24	0.32	190	1.29	0.93
VM10-093	Carb	3574	11.4	13.5	2.83	11.3	2.35	0.53	2.46	0.36	2.14	15.3	0.44	1.19	0.16	1.00	0.14	65.3	0.97	0.59
VM31-152	Carb	4174	8.27	9.18	2.11	8.76	1.87	0.44	2.00	0.30	1.74	11.7	0.35	0.94	0.13	0.79	0.11	48.7	0.92	0.53
VM10-89	Carb	3523	13.2	17.5	3.25	13.1	2.72	0.63	2.86	0.42	2.51	18.1	0.51	1.40	0.19	1.20	0.17	77.8	0.94	0.66
TH1-54S	Carb	3840	26.4	45.9	6.71	26.4	5.44	1.20	5.22	0.77	4.40	27.5	0.87	2.35	0.33	2.06	0.30	156	1.12	0.86
VM20-242	RC†	4565	75.0	139	20.5	81.2	17.5	4.01	17.1	2.56	14.4	75.1	2.76	7.26	1.00	6.21	0.90	465	1.11	0.88
AT180-118P	Carb	4500	34.2	72.5	8.53	31.7	6.23	1.31	5.19	0.78	4.44	23.6	0.87	2.41	0.36	2.38	0.35	195	1.27	1.09
VM20-241	Carb	4372	25.4	48.3	6.47	25.0	5.08	1.12	4.80	0.71	4.11	24.8	0.81	2.22	0.31	2.00	0.29	152	1.12	0.95
VM10-88	RC†	4971	85.3	166	22.1	84.9	17.3	3.90	15.9	2.37	13.8	82.3	2.72	7.48	1.07	6.87	1.01	513	1.11	0.96
AT181-1	Carb	3895	1.22	1.03	0.22	0.94	0.19	0.05	0.25	0.04	0.26	3.40	0.06	0.18	0.02	0.13	0.02	7.8	0.62	0.48
RC21-02	RC	3895	33.3	72.0	8.27	30.8	6.12	1.29	5.16	0.78	4.51	25.3	0.88	2.46	0.36	2.40	0.35	194	1.22	1.12
VM22-212	RC†	6081	62.8	117	18.5	72.3	15.7	3.47	14.0	2.09	11.6	59.0	2.18	5.72	0.79	4.89	0.69	391	1.24	0.85
VM10-87	GC	5329	46.8	101	11.5	42.2	8.15	1.58	6.74	1.00	5.65	29.7	1.08	2.94	0.43	2.84	0.42	262	1.43	1.13
D11805_7-S1	GC	6129	24.1	46.5	5.83	21.8	4.24	0.91	3.78	0.56	3.21	18.9	0.64	1.77	0.26	1.67	0.25	134	1.23	1.01
D11805_7-S2	GC	6129	24.5	47.1	5.86	22.0	4.26	0.91	3.75	0.56	3.22	19.7	0.65	1.79	0.26	1.67	0.25	136	1.23	1.01
D10311-S1	RC	6133	47.1	123	11.4	42.0	8.19	1.74	7.12	1.08	6.28	35.2	1.24	3.49	0.51	3.37	0.51	292	1.19	1.37
D10311-S2	RC	6133	49.6	138	12.1	44.5	8.85	1.88	7.55	1.15	6.61	36.3	1.29	3.55	0.52	3.42	0.51	316	1.24	1.46
D11805_5-S1	GC	5554	23.8	46.1	5.70	21.3	4.13	0.89	3.68	0.54	3.13	19.2	0.62	1.73	0.25	1.62	0.24	133	1.23	1.02
D11805_5-S2	GC	5554	24.0	46.3	5.76	21.5	4.18	0.89	3.70	0.55	3.15	19.1	0.62	1.74	0.25	1.64	0.24	134	1.24	1.01
VM27-255	RC	5554	47.0	117	11.3	41.3	8.01	1.67	6.68	1.02	5.75	30.8	1.11	3.09	0.45	3.00	0.45	278	1.33	1.32
VM32-52	Carb	5220	43.5	110	10.7	39.5	7.81	1.65	6.61	1.01	5.78	31.6	1.13	3.13	0.46	3.00	0.45	267	1.25	1.32
KA74-0046	RC	4838	36.2	73.7	9.21	34.7	6.94	1.53	6.10	0.91	5.10	28.2	0.98	2.63	0.38	2.47	0.36	209	1.30	1.03
VM23-99	Carb	4118	21.4	35.7	5.12	19.7	3.86	0.84	3.55	0.53	3.15	19.8	0.64	1.78	0.26	1.70	0.26	118	1.07	0.86
VM29-170	Carb	4455	19.3	30.9	4.53	17.4	3.42	0.78	3.21	0.47	2.70	16.8	0.54	1.46	0.21	1.32	0.20	103	1.20	0.84
VM30-54	Carb	3506	14.7	25.2	3.53	13.5	2.61	0.57	2.40	0.35	2.04	13.4	0.41	1.15	0.17	1.10	0.17	81.2	1.14	0.89
KM1-046P	GC	1221	11.8	21.3	2.97	11.4	2.14	0.46	1.83	0.26	1.54	10.1	0.32	0.92	0.14	0.92	0.14	66.2	1.15	0.91

[a] Carb = carbonate; RC = red clay; RC† = red clay with micronodules; GC = grey clay. $Ce^* = (2 \times Ce/Ce_{NASC}) / (La/La_{NASC} + Nd/Nd_{NASC})$; $LREE/HREE = (La/La_{NASC} + 2 \times Pr/Pr_{NASC} + Nd/Nd_{NASC}) / (Er/Er_{NASC} + Tm/Tm_{NASC} + Yb/Yb_{NASC} + Lu/Lu_{NASC})$.

Table 5
Concentrations of metals in micronodules.

Sample	Nodule #	Mn wt%	Fe wt%	Ti ppm	Cr ppm	Cu ppm	V ppm	Co ppm	Ni ppm	Ba ppm
VM10-088	1	35.6	5.26	4140	8.67	1630	1110	4330	3700	5640
	2	14.3	1.29	1140	29.2	2450	194	1090	15100	441
	3	11.8	1.59	1320	34.3	1790	195	1400	9890	632
	Avg	12.8	2.43	2710	38.2	1540	389	1550	5450	1480
	SD (n = 14)	10.3	1.19	1920	19.1	952	306	1270	4290	1780
VM20-242	1	30.6	10.5	5870	20.9	953	1560	6900	2480	2390
	2	14.6	6.60	3540	14.7	686	940	2630	1290	1220
	3	19.4	6.50	3660	17.6	746	927	3610	2220	1200
	Avg	24.2	8.50	4950	25.1	844	1210	4610	2050	1610
	SD (n = 49)	21.6	7.13	765	17.1	144	187	1660	426	311
VM25-033	1	14.9	1.48	1080	21.7	1530	209	756	7430	596
	2	16.0	2.40	2700	90.5	1620	390	1870	7570	558
	3	15.3	2.52	2040	40.4	1480	298	1310	6340	544
	Avg	21.1	1.98	1500	38.7	2740	293	1910	15300	665
	SD (n = 86)	7.17	0.77	507	28.9	1250	101	953	8920	167
VM25-032	1	8.26	0.94	1710	32.1	1560	140	116	4890	400
	2	8.50	1.12	1840	38.6	1440	166	143	4520	461
	3	5.90	1.74	2780	108	882	242	202	2980	389
	Avg	7.55	1.16	1940	44.1	1330	161	189	4110	415
	SD (n = 19)	1.91	0.27	455	18.0	467	38.1	123	1210	63.1
VM22-212	1	16.8	1.15	877	29.3	1220	263	2140	8440	935
	2	10.9	1.66	1590	51.4	934	314	1270	5280	624
	3	11.9	6.87	4450	31.1	903	2230	584	1150	4410
	Avg	18.2	1.46	1200	30.8	1290	423	2040	8280	1070
	SD (n = 49)	7.57	1.37	893	16.3	337	453	870	3300	850

(North America Basin), and VM22-212 (Canary Basin). The nodules are Fe-Mn rich, with Mn concentrations up to ~35.6 wt%, and Fe concentrations up to ~10.5 wt%. Micronodules from the Central Atlantic tend to have higher Fe/Mn ratios (~0.3) compared to the other sites (~0.1), higher concentrations of V, Ba and Ti, and lower concentrations of Ni and Cu.

The ΣREY content of the micronodules ranges from ~200 to 3620 ppm. Nodules from sample VM20-242 have highest ΣREY (average = 2710 ppm) while the average ΣREY content of the other samples is lower (VM10-088 = 728 ppm, VM25-033 = 516 ppm, VM25-032 = 248 ppm and VM22-212 = 487 ppm). ΣHREE concentrations range from ~20 to ~200 ppm, and are also much higher in sample VM20-242 (average 162 ppm) than the average of the other samples (18.3 to 31.7 ppm).

Most of the micronodules have positive Ce anomalies; the average Ce anomaly in micronodules from sample VM22-212 (1.14) is slightly lower than it is in the other samples (2.51–8.36). Some of the nodules in sample VM10-088 have negative Ce anomalies (~0.78). Many of the micronodules from samples VM25-033, VM25-032, VM10-088 and VM22-212 are slightly enriched in the MREE (Fig. 8) but this is not true for most of the micronodules from VM20-242. Many of the micronodules from VM20-242 are also depleted in Y relative to Ho, but most of the other micronodules have a positive Y anomaly. Most of the micronodules are slightly enriched in the HREE relative to the LREE (average LREE/HREE = 0.78–0.95) but, on average, micronodules from sample VM25-032 are slightly enriched in the LREE (LREE/HREE = 1.08).

4.3. Factor analysis

To better quantify and understand the processes that control the chemical composition of the sediment samples, the elemental data were subjected to statistical factor analysis (Winters and Buckley, 1992) using the RStudio.Ink Varimax rotation scheme with Kaiser normalisation. The results of this analysis are shown in Tables 7 and 8. Differences in the chemical composition of the sediment samples can be accounted for statistically by changes in the relative proportions of three principal factors (with eigenvalues, or sums of squared (SS) loadings, of >1) which together account for 92% of the sample variance.

Factor 1 is the main factor controlling REY concentrations, with the exception of Ce, and it accounts for 58.3% of the sample variance. Factor 1 also has a high loading for Mn, Co, Ni and Cu, and all of the REY (including Ce) show a significant ($p < 0.05$; Table 8) positive correlation with Mn, Co and Cu and also Fe. Mn, Fe, Cu, Co and Ni are generally considered to have a significant hydrogenous source in deep-sea sediments (e.g. Thomson et al., 1984).

Factor 2 has high loading factors for Na, Al, K, Ti, Fe and Th, and also for Ce. The light REY (La-Nd) have a higher loading in this factor than the heavy REYs, and they show a significant positive correlation with Al, K and Ti ($p > 0.05$; Table 8). Ca has a negative loading in this factor. Factor 2 can be considered to represent the detrital component, and it accounts for the 27.8% of the sample variance.

Factor 3 accounts for the 5.9% of the sample variance. It has an eigenvalue of >1, so it is statistically significant, but no element is dominantly loaded in this factor. However, slightly higher loadings are found for Mn and Co.

5. Discussion

5.1. REY carrier phases in North Atlantic deep-sea sediments

ΣREY concentrations are positively correlated with Al, K and Ti which are enriched in detrital minerals (Table 8), and negatively correlated with elements that are relatively enriched in $CaCO_3$, such as Ca (Tables 7 and 8, Fig. 6). Partitioning of REE, especially LREE, into the carbonate lattice is directly influenced by REE concentrations in seawater (Zhong and Mucci, 1995). Consequently, the REY concentration of carbonates is low relative to detrital minerals and carbonates actively dilute the REY resource in deep-sea sediments (de Lange et al., 1992; Dubinin and Rozanov, 2001; Kato et al., 2011).

However, the relative proportions of detrital vs. carbonate material only accounts for ~28% of the total variance in the chemical composition of the North Atlantic deep-sea sediments, and the factor analysis reveals that the REY are also located in association with Mn, Fe, Cu, Co and Ni

Table 6
Concentrations (ppm) of rare earth elements and yttrium (REY) in micronodules. $Ce^* = (2 \times Ce/Ce_{NASC}) / (La/La_{NASC} + Nd/Nd_{NASC})$; $LREE/HREE = (La/La_{NASC} + 2 \times Pr/Pr_{NASC} + Nd/Nd_{NASC}) / (Er/Er_{NASC} + Tm/Tm_{NASC} + Yb/Yb_{NASC} + Lu/Lu_{NASC})$; $Y/Ho = (Y/Y_{NASC}) / (Ho/Ho_{NASC})$.

Sample	Nodule #	La	Ce	Pr	Nd	Sm	Eu	Gd	Tb	Dy	Y	Ho	Er	Tm	Yb	Lu	ΣREY	LREE/HREE	Ce^*	Y/Ho
VM10-088	1	48.8	2440	5.58	20.6	3.54	0.90	5.22	0.60	4.29	15.8	0.92	3.11	0.49	4.34	0.83	2560	0.64	36.2	0.81
	2	49.2	99.9	12.0	46.6	9.98	2.50	9.19	1.57	10.5	60.4	1.92	6.03	0.92	5.71	0.84	317	0.74	1.03	1.48
	3	77.5	140	20.3	97.8	21.8	4.52	19.7	2.99	18.6	118	3.86	11.4	1.53	10.4	1.35	550	0.75	0.78	1.43
	Avg.	46.4	542	10.6	42.7	9.30	2.01	8.68	1.29	7.87	44.8	1.53	4.61	0.66	4.41	0.68	728	0.89	8.36	1.32
	SD (n = 14)	14.8	797	4.59	21.4	5.11	1.05	4.48	0.71	4.08	27.0	0.81	2.35	0.30	1.87	0.24	761	0.16	13.3	0.23
VM20-242	1	413	2500	60.6	235	45.0	10.9	50.8	8.24	51.6	168	10.1	29.8	4.54	30.0	4.75	3620	0.84	3.92	0.78
	2	223	1280	33.3	128	25.8	5.97	31.3	4.70	30.7	106	5.79	17.1	2.53	16.9	2.69	1910	0.81	3.70	0.86
	3	244	1460	37.1	150	30.1	7.70	34.8	5.24	33.6	125	6.83	20.6	3.12	20.3	3.39	2180	0.74	3.75	0.86
	Avg.	314	1827	45.1	181	36.4	8.23	41.4	6.37	41.2	144	8.14	24.4	3.61	24.7	4.05	2710	0.78	3.80	0.84
	SD (n = 49)	63.6	407	8.28	32.2	6.65	1.41	7.43	1.21	7.65	24.7	1.58	4.72	0.72	4.82	0.80	560	0.04	0.25	0.06
VM25-033	1	49.5	234	12.7	58.4	14.0	3.24	15.0	2.05	11.9	69.4	2.49	7.01	0.78	4.70	0.65	486	0.89	2.13	1.31
	2	52.0	263	16.0	58.1	17.7	3.40	13.8	2.22	12.4	63.7	2.44	6.85	0.71	4.86	0.67	518	1.01	2.35	1.22
	3	42.0	401	8.31	33.1	7.11	1.73	8.03	1.14	7.25	32.1	1.25	3.89	0.61	4.28	0.64	552	0.78	5.34	1.20
	Avg.	40.2	346	9.91	39.3	9.01	1.97	8.92	1.29	8.08	40.1	1.56	4.50	0.61	3.87	0.58	516	0.95	4.20	1.22
	SD (n = 86)	11.3	123	3.71	15.8	3.98	0.90	4.29	0.63	3.92	19.9	0.72	1.95	0.24	1.35	0.19	144	0.17	1.18	0.15
VM25-032	1	25.5	127	5.00	20.1	4.06	0.83	3.84	0.64	3.65	17.7	0.77	2.22	0.27	1.76	0.31	214	0.98	2.80	1.08
	2	30.0	137	5.44	18.6	4.72	0.94	3.60	0.61	3.32	17.4	0.62	1.89	0.29	1.66	0.18	226	1.24	2.84	1.33
	3	47.1	158	12.2	56.4	12.6	2.45	12.0	1.49	8.86	41.4	1.52	4.25	0.59	3.72	0.54	363	1.18	1.50	1.28
	Avg.	29.9	138	6.50	26.4	5.76	1.18	5.39	0.81	4.58	23.4	0.88	2.54	0.36	2.24	0.35	248	1.08	2.51	1.25
	SD (n = 19)	6.20	21.0	1.83	8.30	1.94	0.36	1.90	0.25	1.37	7.40	0.27	0.75	0.13	1.03	0.17	42.0	0.20	0.43	0.10
VM22-212	1	30.5	135	8.95	33.6	7.68	1.65	7.23	0.95	6.11	29.2	1.12	3.91	0.43	2.99	0.51	270	0.93	2.08	0.87
	2	26.5	116	5.47	21.6	4.43	0.95	4.61	0.69	3.56	16.3	0.70	2.50	0.30	2.21	0.29	206	0.95	2.40	0.54
	3	209	1620	55.9	242	51.0	10.8	57.2	7.75	46.4	154	9.47	26.6	3.59	20.1	3.17	2520	0.89	3.53	0.76
	Avg.	30.4	201	7.80	32.1	7.10	1.51	7.19	1.02	6.14	24.4	1.23	3.58	0.48	3.08	0.46	487	0.87	1.14	1.03
	SD (n = 49)	43.7	345	11.8	51.3	10.7	2.27	12.2	1.64	9.84	32.0	2.01	5.63	0.76	4.15	0.67	533	1.27	1.54	0.12

Table 7
Varimax rotated factor matrix for North Atlantic deep-sea sediments. Numbers in bold denote elements that appear to be loaded in the factor.

	Factor 1	Factor 2	Factor 3
Na	0.229	**0.680**	
Al	0.420	**0.878**	0.179
K	0.359	**0.906**	0.146
Ca	−0.421	**−0.871**	−0.163
Ti	0.447	**0.859**	
Mn	**0.787**	0.160	0.590
Fe	0.674	**0.684**	0.227
Co	**0.755**	0.208	0.605
Ni	**0.683**	0.230	0.326
Cu	**0.803**	0.291	0.414
La	**0.822**	0.533	0.134
Ce	0.597	**0.674**	0.322
Pr	**0.863**	0.474	0.136
Nd	**0.886**	0.432	0.135
Sm	**0.909**	0.382	0.147
Eu	**0.931**	0.325	0.151
Gd	**0.942**	0.293	0.149
Tb	**0.939**	0.302	0.155
Dy	**0.941**	0.300	0.149
Y	**0.962**	0.243	
Ho	**0.943**	0.298	0.144
Er	**0.937**	0.318	0.139
Tm	**0.923**	0.354	0.138
Yb	**0.908**	0.387	0.134
Lu	**0.896**	0.407	0.141
Th	0.414	**0.825**	0.259
U	0.492	−0.117	−0.169
Eigen value (SS loading)	15.75	7.50	1.59
Total variance (%)	58.3	27.8	5.9
Acum. variance (%)	58.3	86.1	92

(Tables 7 and 8) that are generally considered to have a significant hydrogenous source in deep-sea sediments (e.g. Thomson et al., 1984).

REY distribution patterns for the red clays show a mirror image of the seawater distribution pattern, with LREE enrichment relative to the HREE and a positive Ce anomaly (Fig. 4). This supports the idea that the red clays acquire at least part of their REY from seawater (Thomson et al., 1984; Dubinin and Rozanov, 2001; Kato et al., 2011). The red clays are also enriched in other elements that have a hydrogenous source (e.g. Fe, Mn, Cu, Co, Ni and V: Turekian and Imbrie, 1966; Chester and Messiha-Hanna, 1970; Thomson et al., 1984) relative to NASC (Fig. 5). Significant enrichment of the REY in red clays, due to input of hydrogenous material, has also been noted in the Brazil Basin (Dubinin and Rimskaya-Korsakova, 2011), and for mesopelagic clays from the western part of the North Equatorial Pacific (Dubinin and Uspenskaya, 2006).

By contrast, REY distribution patterns for the grey clays are closer to shale, though they are slightly depleted in the HREE possibly because our dissolution procedure underestimated the contribution of refractory minerals (Sholkovitz, 1990). Although they are slightly enriched in Mn relative to NASC, they show no enrichment in other metals that have a hydrogenous source (Fig. 5). This supports the idea that the REYs in grey clays are dominated by terrigenous input because they are deposited relatively rapidly and therefore contain an insignificant hydrogenous component (Thomson et al., 1984).

REY distribution patterns for the carbonate-rich sediments are similar to the seawater pattern, with enrichment of the HREE relative to the LREE, a negative Ce anomaly and a positive Ho anomaly (Fig. 4). The HREE are relatively enriched in seawater because they form stable complexes with CO_3^{2-} compared to the LREE (Cantrell and Byrne, 1987; Lee and Byrne, 1992). Carbonates that precipitate from seawater inherit the REY distribution pattern, and ancient carbonates can provide important information about palaeoceanographic environments (e.g. Nagarajan et al., 2011).

Uptake of REY from seawater is widely considered to occur via scavenging by Fe-Mn (oxyhdr)oxide phases (Piper, 1974; Li, 1981; German et al., 1991; De Carlo and Green, 2002; Dubinin and Rimskaya-Korsakova, 2011; Bau and Koschinsky, 2009). Sequential leaching of suspended particles reveals that REE concentrations are high in Mn oxides (Sholkovitz et al., 1994), but also in hydrous Fe oxides (Bau and Koschinsky, 2009), which is consistent with analyses of suboxic porewaters in sediments from the Peru and California margins that show the REYs are released during reduction of Fe-oxides, but not Mn-oxides (Haley et al., 2004). Our data for North Atlantic deep-sea sediments supports the participation of both Mn- and Fe-(oxyhydr)oxide phases and, furthermore, they indicate that the LREE and HREE show a greater affinity for Fe-oxides whereas, in general, the MREE appear to have a greater affinity for Mn-oxide phases (Table 8).

5.2. Accumulation of REYs in micronodules

Fe-Mn rich micronodules are common in pelagic sediments, and they are morphologically, mineralogically and chemically similar to larger Fe-Mn nodules found at the sediment surface in sediment-starved deep-ocean basins (Addy, 1979; Dubinin and Sval'nov, 2003; Pattan et al., 1994; Sval'nov et al., 1991). Micronodules can have a hydrogenous, diagenetic, or hydrothermal source. Hydrogenous micronodules precipitate from seawater, whereas diagenetic nodules form from metal ions in sub-oxic pore waters, and hydrothermal nodules form from metals supplied by hydrothermal vent fluids. These different types of nodule can be distinguished by the field on which they plot on a Mn-Fe-(Ni + Co + Cu) ternary diagram (Bonatti et al., 1972) (Fig. 7), which delimitates the diagenetic, hydrogenous and hydrothermal fields according to the relative proportions of these groups of elements. According to this, hydrogenous deposits will show higher Fe/Mn ratios, and lower (Ni + Co + Cu) than diagenetic nodules, whereas hydrothermal nodules will have the lowest (Ni + Co + Cu) content.

Most of the micronodules in deep-sea North Atlantic red clays have a diagenetic or mixed (hydrogenous and diagenetic) source (Fig. 7), but micronodules from sample VM20-242, and some micronodules from sample VM10-088, have a mainly hydrogenous source. None of the sediment samples appear to contain micronodules with a hydrothermal signature, even though some of the micronodule-containing sediments (VM20-242 and VM10-88) were from close to the Mid-Atlantic Ridge.

REY distribution patterns (Fig. 8) shows that the hydrogenous micronodules (e.g. from sample VM20-242) have higher ΣREY and Nd concentrations than the diagenetic micronodules, which is consistent with data compiled by Bau et al. (2014) for regular Fe-Mn nodules. This, together with the positive Ce anomalies is indicative of a hydrogenous origin for these nodules (Piper, 1974; Addy, 1979; de Lange et al., 1992; Nath et al., 1992; Kasten et al., 1998). However, the same authors report that diagenetic nodules are characterised by no or negative Ce anomalies, whereas most of our micronodules have small positive Ce anomalies. This may indicate that the 'diagenetic' micronodules also contain a small hydrogenous component.

Y is depleted with respect to its geochemical twin Ho in most micronodules from sample VM20-242 and some from VM10-088 and VM22-212. Y^{3+} and Ho^{3+} have very similar ionic radii, but Y forms less stable surface complexes, so Ho is preferentially scavenged by metal (oxyhydr)oxide phases (Bau et al., 1995, 1996, 1997; Bau and Dulski, 1999; Schijf and Marshall, 2011). Thus, hydrogenous nodules can be expected to be enriched in Ho. By contrast, micronodules from sample VM25-032 and most micronodules from VM25-033 and VM10-088 have shale-normalised Y/Ho ratios ≥1, as is typical for seawater (Douville et al., 1999). Positive Y anomalies are usually characteristic of hydrothermal Fe-Mn nodules, or nodules that have become phosphatized (Bau et al., 2014). While we did not assess the P content of the micronodules, as discussed above we see no evidence for a hydrothermal signature on the basis of their (Cu + Ni + Co) content (Fig. 8). However, sequential leaching experiments on Fe-Mn crusts have shown

Table 8
Correlation coefficients between elements in deep Atlantic sediments. Significant ($p < 0.05$) correlations are highlighted in bold.

	Na	Al	K	Ca	Ti	Mn	Fe	Co	Ni	Cu	La	Ce	Pr	Nd	Sm	Eu	Gd	Tb	Dy	Y	Ho	Er	Tm	Yb	Lu	Th	U
Na																											
Al	0.68																										
K	0.71	**0.97**																									
Ca	−0.69	**−0.97**	**−0.97**																								
Ti	0.67	**0.96**	**0.93**	**−0.94**																							
Mn	0.31	0.57	0.51	−0.57	0.51																						
Fe	0.62	**0.92**	**0.90**	**−0.91**	**0.89**	**0.77**																					
Co	0.34	0.61	0.56	−0.60	0.55	**0.98**	**0.79**																				
Ni	0.51	0.51	0.48	−0.53	0.45	**0.78**	0.70	0.71																			
Cu	0.50	0.66	0.60	−0.64	0.63	**0.92**	**0.85**	**0.91**	**0.83**																		
La	0.54	**0.85**	**0.80**	**−0.84**	**0.84**	**0.81**	**0.94**	**0.82**	0.68	**0.87**																	
Ce	0.59	**0.92**	**0.88**	**−0.90**	**0.89**	**0.76**	**0.93**	**0.80**	0.57	**0.82**	**0.93**																
Pr	0.52	**0.81**	**0.77**	**−0.80**	**0.80**	**0.83**	**0.94**	**0.84**	0.71	**0.88**	**0.99**	**0.90**															
Nd	0.49	**0.78**	0.74	**−0.78**	**0.77**	**0.84**	**0.92**	**0.85**	0.72	**0.89**	**0.99**	**0.88**	**1.00**														
Sm	0.47	0.74	0.70	−0.74	0.73	**0.86**	**0.91**	**0.86**	0.74	**0.90**	**0.97**	**0.85**	**0.99**	**1.00**													
Eu	0.44	0.70	0.66	−0.70	0.70	**0.87**	**0.89**	**0.86**	**0.75**	**0.90**	**0.96**	**0.83**	**0.98**	**0.99**	**1.00**												
Gd	0.42	0.68	0.63	−0.68	0.68	**0.88**	**0.87**	**0.87**	**0.75**	**0.90**	**0.95**	**0.81**	**0.98**	**0.98**	**0.99**	**1.00**											
Tb	0.43	0.69	0.64	−0.69	0.68	**0.88**	**0.87**	**0.87**	**0.75**	**0.90**	**0.95**	**0.82**	**0.98**	**0.99**	**0.99**	**1.00**	**1.00**										
Dy	0.43	0.69	0.63	−0.68	0.68	**0.88**	**0.87**	**0.87**	**0.75**	**0.90**	**0.95**	**0.81**	**0.98**	**0.99**	**0.99**	**1.00**	**1.00**	**1.00**									
Y	0.39	0.64	0.57	−0.63	0.65	**0.85**	**0.83**	**0.83**	0.74	**0.89**	**0.94**	**0.78**	**0.96**	**0.97**	**0.98**	**0.99**	**0.99**	**0.99**	**0.99**								
Ho	0.42	0.68	0.63	−0.68	0.69	**0.87**	**0.87**	**0.86**	**0.76**	**0.90**	**0.95**	**0.81**	**0.98**	**0.98**	**0.99**	**1.00**	**1.00**	**1.00**	**1.00**	**0.99**							
Er	0.44	0.70	0.64	−0.69	0.70	**0.87**	**0.88**	**0.86**	**0.75**	**0.90**	**0.96**	**0.82**	**0.98**	**0.99**	**0.99**	**1.00**	**1.00**	**1.00**	**1.00**	**0.99**	**1.00**						
Tm	0.45	0.73	0.67	−0.72	0.73	**0.86**	**0.89**	**0.85**	**0.75**	**0.90**	**0.97**	**0.84**	**0.98**	**0.99**	**0.99**	**0.99**	**0.99**	**1.00**	**0.99**	**0.99**	**1.00**	**1.00**					
Yb	0.47	**0.75**	0.69	−0.74	**0.76**	**0.85**	**0.90**	**0.85**	0.74	**0.90**	**0.98**	**0.86**	**0.99**	**0.99**	**0.99**	**0.99**	**0.99**	**0.99**	**0.99**	**0.99**	**0.99**	**1.00**	**1.00**				
Lu	0.48	**0.76**	0.70	**−0.75**	**0.77**	**0.85**	**0.91**	**0.85**	0.73	**0.90**	**0.98**	**0.87**	**0.99**	**0.99**	**0.99**	**0.98**	**0.98**	**0.98**	**0.98**	**0.98**	**0.99**	**0.99**	**1.00**	**1.00**			
Th	0.65	**0.97**	**0.93**	**−0.94**	**0.93**	0.61	**0.88**	0.65	0.49	0.68	**0.85**	**0.96**	**0.81**	**0.78**	0.73	0.69	0.67	0.68	0.68	0.63	0.68	0.69	0.72	0.74	**0.76**		
U	0.41	0.38	0.41	−0.42	0.37	−0.02	0.25	0.01	0.03	0.06	0.19	0.22	0.17	0.15	0.12	0.10	0.08	0.08	0.08	0.06	0.08	0.10	0.12	0.13	0.15	0.30	

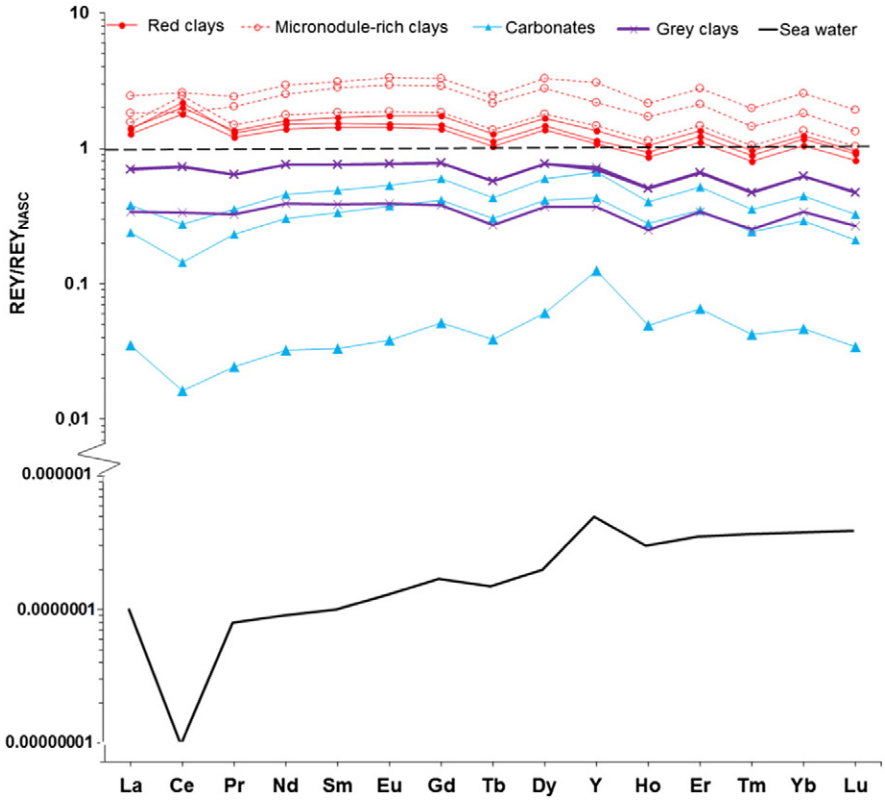

Fig. 4. REY distribution patterns, normalised to North America Shale Composite (NASC; Gromet et al., 1984), for North Atlantic deep-sea sediments and comparison with a sea water-like pattern (Douville et al., 1999). Three representative samples from each sediment type are shown. The REY distribution pattern for deep Atlantic seawater is also shown for comparison (Douville et al., 1999). Black dashed line shows values for NASC; samples with REY/REY$_{NASC}$ > 1 are enriched in the REY relative to NASC; samples with REY/REY$_{NASC}$ < 1 are depleted in the REY relative to NASC.

that Mn-oxides have shale-normalised Y/Ho ratios of ≥1 whereas Fe-oxides have negative Y anomalies (Bau and Koschinsky, 2009); in this connection, micronodules with shale-normalised Y/Ho ratios of >1 tend to have higher Mn/Fe (Mn/Fe > ~5). Thus, the positive Y anomaly in the micronodules with high Mn/Fe may suggest that REY scavenging from ambient seawater by Mn-oxides is very rapid and produces a disequilibrium REY distribution (Bau et al., 2014).

There is a positive correlation between the Fe and Mn content of the micronodules and ΣREY (Fig. 9). However, the diagenetic nodules, which have higher Mn relative to Fe (~10, compared to ~4.5 in hydrogenous nodules), have lower ΣREY. Although some studies suggest that diagenetic nodules have low ΣREY concentrations because of REY loss due to dissolution of Fe- and Mn-(oxyhydr)oxide carrier phases (Nath et al., 1992), we note that the diagenetic nodules in the North Atlantic deep-sea clays have similar Mn concentrations to the hydrogenous nodules, although the hydrogenous nodules have higher Fe. The hydrogenous micronodules are also enriched in V and Co, and depleted in Cu and Ni, compared to the diagenetic nodules. In a study of ferromanganese micronodules in sediments in the northeast Pacific basin (Dubinin et al., 2008), two populations of micronodules were found, one relatively enriched in Mn, Ni and Cu and depleted in Fe, in Ce and Co, which is suggested to form under suboxic conditions, and the other with higher concentrations of Fe, ΣREY (especially Ce) and Co, but similar Mn, that formed under oxic conditions.

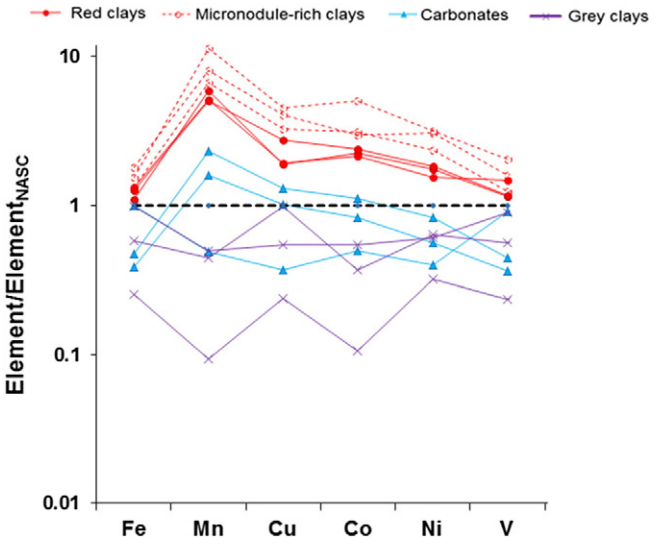

Fig. 5. Distribution of transition metals in North Atlantic deep-sea sediments relative to NASC. Black dashed line shows values for NASC.

Although some of the micronodule-rich sediments were collected in close proximity to the Mid-Atlantic Ridge, the micronodules do not appear to contain a significant hydrothermal component (Fig. 7), which supports the conclusions of previous studies conducted in the North Atlantic (Dubinin and Rozanov, 2001). This may be because hydrothermal plumes tend to be confined to the axial valley due to the topography of slow spreading ridges (e.g. Charlou and Donval, 1993). By contrast, in the Pacific Ocean, hydrothermal sediments can be found several hundreds of kilometres away from the fast-spreading East Pacific Rise (Dymond, 1981).

5.3. Comparison between Atlantic and Pacific deep-sea sediments

On average, the total REY abundances for our North Atlantic deep-sea sediments (ΣREY up to 512 ppm) are lower than reported values for the Pacific (ΣREY up to 2230 ppm) (de Baar et al., 1985; Kato et al., 2011). This difference is likely to be, in part, due to differences in

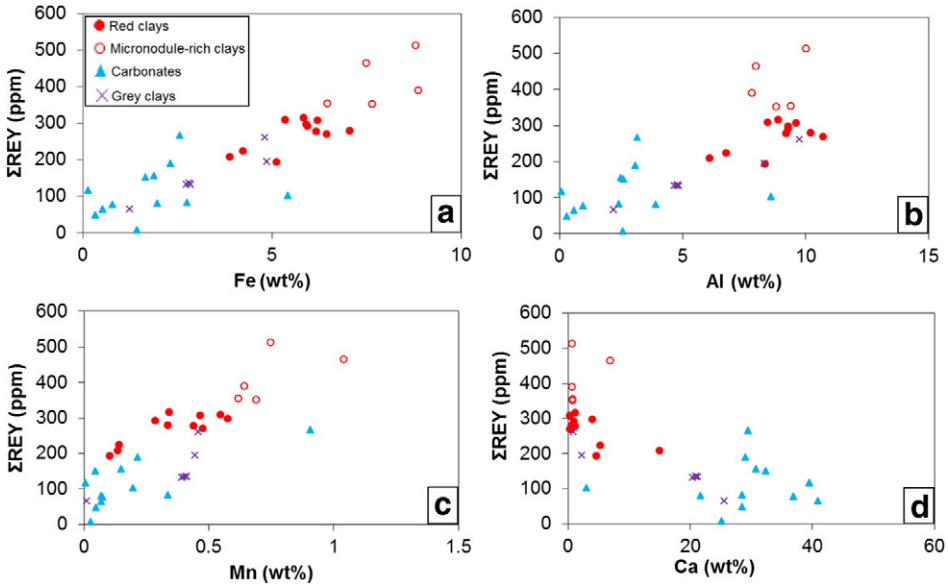

Fig. 6. Relationship between ΣREY content and (a) Fe, (b) Al, (c) Mn and (d) Ca in North Atlantic deep-sea sediments. Note that the micronodule-rich red clays are enriched in Fe and Mn, as well as the REY.

sedimentation rate; in general, sedimentation rates are higher in the Atlantic as most of the seafloor lies above the carbonate compensation depth (Sverdrup et al., 1970; Berger, 1975; Biscaye et al., 1976). The REY content of the deep-sea clays is principally controlled by scavenging of the REYs from seawater, so the lower the sedimentation rate, the greater the uptake of the REY during sedimentation. Differences in sediment lithology could also be a factor; in the Pacific, deep-sea sediments are often rich in fish bone debris which is composed of biogenic calcium phosphate that readily accumulates REYs from seawater (Toyoda et al., 1990; Dubinin and Rozanov, 2001; Dubinin, 2004). Similarly, widely distributed iron and manganese oxyhydroxides of hydrothermal origin in the Pacific scavenge dissolved phosphate (Feely et al., 1996); in deep-sea sediments this P is converted to calcium-iron hydroxophosphates that have high REY concentrations (Dubinin, 2001). The REY content of the clays may also be affected by differences in the REY concentration of seawater. REY concentrations are higher in the deep Pacific than they are in the deep Atlantic, partly because of dissolution of sinking biogenic particles from surface waters (de Baar et al., 1985), and partly because deep Pacific waters have lower carbonate ion concentrations which enhances uptake of the REY onto particle surfaces (Sholkovitz, 1995; Byrne, 2002; Luo and Byrne, 2004).

Although the North Atlantic deep-sea clays have lower REY contents than in the Pacific, they have a much more pronounced Ce anomaly (up to 2.4 in the Atlantic, compared to up to 1.4 in the Pacific; Toyoda et al., 1990). It is likely that this is related to higher levels of bottom water oxygenation in the Atlantic than in the Pacific, which lies at the end of the ocean conveyor (Reid, 1997; Mantyla and Reid, 1983).

5.4. Resource potential of Atlantic deep-sea sediments

The average ΣREY content of the red clay samples analysed in this study is 257 ± 86 ppm (Table 9). Given a dry bulk density of 0.65 g cm^{-3} (Thomson et al., 1984), and assuming that mining will remove the upper ~1 m of seafloor sediments (based on specifications for the Nautilus Minerals seafloor mining tool; Coffey Natural Systems, 2008), 1 km^2 of red clay in the North Atlantic Ocean has the potential to yield 167 ± 56 t of REY oxides (Table 9). This represents a < 1% of the global annual consumption of the REY in 2010 (105,000 t; Hatch, 2012). Similarly, mining of 1 km^2 of grey clay (which has an average ΣREY content of 130 ± 61 ppm (Table 9), will yield 85 ± 40 t of REY oxides.

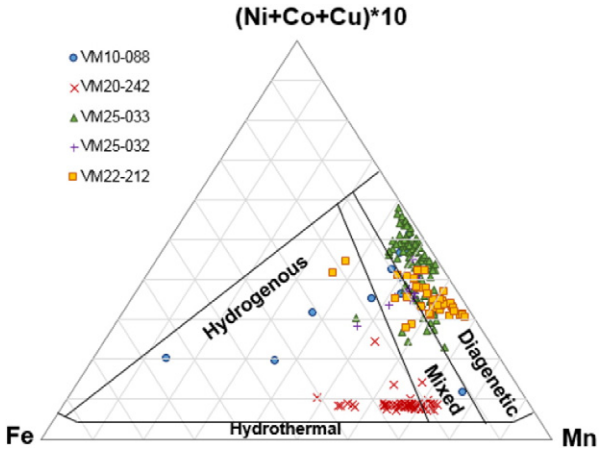

Fig. 7. Ratio of Fe:Mn:Cu + Ni + Co in micronodules from red clay sediments in the North Atlantic,. Black lines define different nodule fields, according to Bonatti et al. (1972) and Wegorzewski and Kuhn (2014).

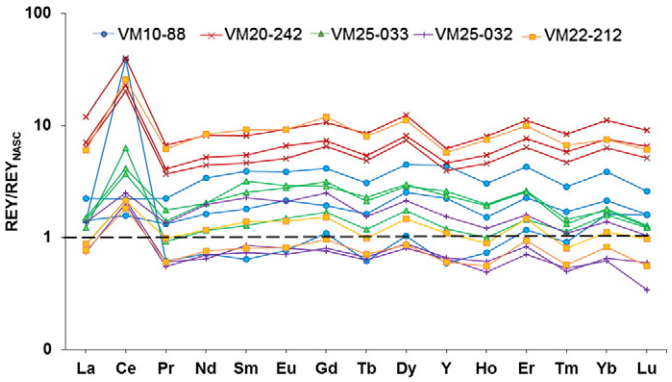

Fig. 8. REY distribution patterns, normalised to NASC for 3 representative micronodules from red clay samples VM20-242, VM10-088, VM22-212 and VM25-033.

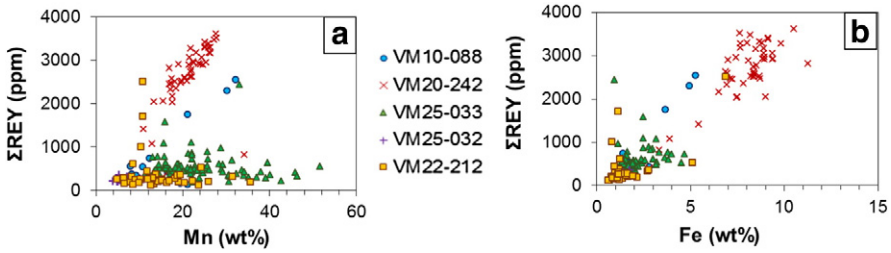

Fig. 9. Relationship between ΣREY content and (a) Fe and (b) Mn in micronodules recovered from North Atlantic deep-sea sediments.

Table 9
Average ΣREY content of North Atlantic deep sea sediments, compared to deep sea clays from the Pacific Ocean.

Area/sediment type	Av. ΣREY content	Mass REY oxides[a]	Mining area[b]	Reference
	ppm	Tonnes/km^2	km^2 yr^{-1}	
North Atlantic red clay	257	167	63	This study
North Atlantic grey clay	130	84.5	124	This study
Eastern South Pacific red clay	1180	767	17	Kato et al. (2011)
Central North Pacific red clay	640	416	32	Kato et al. (2011)

[a] Assumes removal of upper 1 m of sediment, and dry bulk density of 0.65 g cm^{-3}.
[b] Area of seafloor to be mined per year to meet 10% of the global annual REY demand.

The area of North Atlantic red clay (~1 m thick) required to provide ~10% of the global annual demand for the REYs is of the order of ~60 km^2. This is a tiny fraction (<0.0001%) of the total area of the Atlantic Ocean seafloor, but is nevertheless much greater than the area of seafloor calculated to produce the same quantity of REYs in the eastern South Pacific (~1.5 km^2; for an average clay thickness of 10 m) or the central North Pacific (~0.5 km^2; for an average clay thickness of 70 m) (Kato et al., 2011).

As Kato et al. (2011) estimate seafloor REE resources for far greater depths of sediment removal than we assume in this study, the areal extent of sediment extraction required to meet 10% of the global annual demand for a sediment depth of 1 m is provided for comparison with our study in Table 9. Whatever thickness of sediment is removed, it is clear from Table 9 that the higher ΣREY content of Pacific red clays means that the area of seafloor impacted by mining will be less than it is in the Atlantic Ocean. Nevertheless, we caution that mining will almost certainly result in long-term changes to the ecosystem structure, functions and services in the deep sea (e.g. Miljutin et al., 2011) that will extend far beyond the area of sediment removal (Jankowski and Zielke, 2001).

6. Conclusions

Geochemical analyses of a suite of deep-sea sediments from a transect across the North Atlantic at ~24°N indicates that the REY are enriched in slowly-deposited red clays from the Nares Abyssal Plain and the Canary Basin, with highest concentrations found in red clays that contain micronodules of ferromanganese oxides (up to 513 ppm ΣREY). Grey clays that contain significant terrigenous material transported by turbidites contain lower ΣREY (~150 ppm), and carbonate-rich sediments contain lowest ΣREY concentrations (~120 ppm). REY distribution patterns of the red clays mirror that of seawater, with positive Ce anomalies and enrichment in the LREE relative to the HREE. Compared to NASC, the red clays are also enriched in Fe, Mn, Cu, Co, Ni and V, which are typically associated with hydrogenous material. Results of factor analysis confirm that the red clays acquire REY from seawater.

In situ analysis of individual micronodules confirms that they have very high ΣREY (up to 3620 ppm). The micronodules consist of two distinct groups: one with relatively high Fe/Mn and higher V and Co concentrations, and one with relatively lower Fe/Mn and higher Cu and Ni concentrations. The former group appears to have a mostly hydrogenous source, while the latter group has a stronger diagenetic source. The hydrogenous micronodules have highest ΣREY and are significantly enriched in Ce relative to La and Nd (Ce* up to 36.2).

Total REY concentrations in North Atlantic deep-sea sediments are lower than those measured in Pacific deep-sea sediments, by a factor of ~4. This may, in part, be due to overall lower sedimentation rates, higher concentrations of fish bone debris and ferromanganese oxyhydroxides of hydrothermal origin, and higher seawater REY concentrations, in the Pacific. Because of its lower ΣREY concentrations, the area of the seafloor impacted by future mining of deep-sea sediments will be greater in the Atlantic than it would be in the Pacific.

Acknowledgements

This work was funded by the European Union Seventh Framework Programme (FP7/2007-2013) under the MIDAS project, grant agreement no. 603418. The authors wish to thank the curators Dr. Suzanne MacLachlan and Nichole A. Arnest from, respectively, the British Ocean Sediment Core Research Facility (BOSCORF), and the Lamont-Doherty Earth Observatory (LDEO) for their guidance and support in the collection of sediment samples. We also thank Dr. Matthew Cooper and Dr. J. Andy Milton (University of Southampton) for training and technical support for geochemical analyses.

References

Addy, S.K., 1979. Rare earth element patterns in manganese nodules and micronodules from Northwest Atlantic. Geochim. Cosmochim. Acta 43, 1105–1115.
Alonso, E., Sherman, A.M., Wallington, T.J., Everson, M.P., Field, F.R., Roth, R., Kirchain, R.E., 2012. Evaluating rare earth element availability: a case with revolutionary demand from clean technologies. Environ. Sci. Technol. 46 (6), 3406–3414.
Bau, M., Dulski, P., 1999. Comparing yttrium and rare earths in hydrothermal fluids from the mid-Atlantic ridge: implications for Y and REE behaviour during near-vent mixing and for the Y/Ho ratio of Proterozoic seawater. Chem. Geol. 155, 77–90.
Bau, M., Koschinsky, A., 2009. Oxidative scavenging of cerium on hydrous Fe oxide: evidence from the distribution of rare earth elements and yttrium between Fe oxides and Mn oxides in hydrogenetic ferromanganese crusts. Geochem. J. 43, 37–47.
Bau, M., Dulski, P., Möller, P., 1995. Yttrium and holmium in South Pacific seawater: vertical distribution and possible fractionation mechanisms. Chem. Erde 55, 1–15.
Bau, M., Koschinsky, A., Dulski, P., Hein, J.R., 1996. Comparison of the partitioning behaviours of yttrium, rare earth elements, and titanium between hydrogenetic marine ferromanganese crusts and seawater. Geochim. Cosmochim. Acta 60, 1709–1725.

Bau, M., Möller, P., Dulski, P., 1997. Yttrium and lanthanides in eastern Mediterranean seawater and their fractionation during redox-cycling. Mar. Chem. 56, 123–131.
Bau, M., Schmidt, K., Koschinsky, A., Hein, J., Kuhn, T., Usui, A., 2014. Discriminating between different genetic types of marine ferro-manganese crusts and nodules based on rare earth elements and yttrium. Chem. Geol. 381, 1–9.
Berger, W.H., 1975. Deep-Sea Carbonates: Dissolution Profiles from Foraminiferal Calcite. In: Sliter, W.V., Bé, A.W.H., Berger, W.H. (Eds.), Dissolution in Deep-Sea Carbonates. Cushman Found 13. Foraminiferal Research Special Publication, pp. 82–86.
Biscaye, P.E., Kolla, V., Turekian, K.K., 1976. Distribution of calcium carbonate in surface sediments of the Atlantic Ocean. J. Geophys. Res. 81, 2595–2603.
Bonatti, E., Kraemer, T., Rydell, H., 1972. Classification and Genesis of Submarine Iron–Manganese Deposits. In: Horn, D.R. (Ed.), Papers from a Conference on Ferromanganese Deposits on the Ocean Floor. National Science Foundation, pp. 149–166.
Byrne, R.H., 2002. Inorganic speciation of dissolved elements in seawater: the influence of pH on concentration ratios. Geochem. Trans. 2 (2), 11.
Cantrell, K.J., Byrne, J.H., 1987. Rare earth element complexation by carbonate and oxalate ions. Geochim. Cosmochim. Acta 51, 597–605.
Castor, S.B., Hedrick, J.B., 2006. Rare Earth Elements. Industrial Minerals Volume. Society for Mining, Metallurgy, and Exploration, Littleton, Colorado, 7th edition, pp. 769–792.
Charlou, J.L., Donval, J.P., 1993. Hydrothermal methane venting between 12° and 26°N along the mid-Atlantic ridge. J. Geophys. Res. 98, 9625–9642.
Chester, R., Messiha-Hanna, R.G., 1970. Trace element partition patterns in North Atlantic deep-sea sediments. Geochimica et Comochimica Acta 34, 1121–1128.
Coffey Natural Systems, 2008. Solwara 1 Project Environmental Impact Assessment. Nautilus Minerals Niugini Limited.
Cordier, D., 2011. Rare Earths, Mineral Commodity Summary. United States Geological Survey.
de Baar, H.J.W., Bacon, M.P., Brewer, P.G., 1985. Rare earth elements in the Pacific and Atlantic oceans. Geochim. Cosmochim. Acta 49, 1943–1959.
De Carlo, E.H., Green, W.J., 2002. Rare earth elements in the water column of Lake Vanda, McMurdo dry valleys, Antarctica. Geochim. Cosmochim. Acta 66, 1323–1333.
de Lange, G.J., van Os, B., Poorter, R., 1992. Geochemical composition and inferred accretion rates of sediments and manganese nodules from a submarine hill in the Madeira abyssal plain, eastern North Atlantic. Mar. Geol. 109, 171–194.
Douville, E., Bienvenu, P., Charlou, J.L., Donval, J.P., Fouquet, Y., Appriou, P., Gamo, T., 1999. Yttrium and rare earth elements in fluids from various deep-sea hydrothermal systems. Geochim. Cosmochim. Acta 63, 627–643.
Dubinin, A.V., 2001. Geochemistry of iron–calcium hydroxophosphates in pelagic sediments: origin and compositional evolution in the course of diagenesis. Geochem. Int. 39, 585–596.
Dubinin, A.V., 2004. Geochemistry of rare earths in the ocean. Lithol. Miner. Resour. 39, 289–307.
Dubinin, A.V., Rimskaya-Korsakova, M.N., 2011. Geochemistry of rare earth elements in bottom sediments of the Brazil Basin, Atlantic Ocean. Lithol. Miner. Resour. 46, 1–16.
Dubinin, A.V., Rozanov, A.G., 2001. Geochemistry of rare earth elements and thorium in sediments and ferromanganese nodules of the Atlantic Ocean. Lithol. Miner. Resour. 36, 268–279.
Dubinin, A.V., Sval'nov, V.N., 2003. Geochemistry of the manganese ore process in the ocean: evidence from rare earth elements. Lithol. Miner. Resour. 38, 91–100.
Dubinin, A.V., Uspenskaya, T.Y., 2006. Geochemistry and specific features of manganese ore formation in sediments of oceanic bioproductive zones. Lithol. Miner. Resour. 41, 1–14.
Dubinin, A.V., Sval'nov, V.N., Uspenskaya, T.Y., 2008. Geochemistry of the authigenic ferromanganese ore formation in sediments of the Northeast Pacific Basin. Lithol. Miner. Resour. 43, 99–110.
Dymond, J., 1981. Geochemistry of Nazca plate surface sediments — an evaluation of hydrothermal, biogenic, detrital and hydrogenous sources. Geological Society of America Memoir 154, 133–173.
Feely, R.A., Baker, E.T., Marumo, K., Urabe, T., Ishibashi, J., Gendron, J., Lebon, G.T., Okamura, K., 1996. Hydrothermal plume particles and dissolved phosphate over the superfast-spreading southern East Pacific rise. Geochim. Cosmochim. Acta 60 (13), 2297–2323.
German, C.R., Holliday, B.P., Elderfield, H., 1991. Redox cycling of rare earth elements in the suboxic zone of the Black Sea. Geochim. Cosmochim. Acta 55, 3553–3558.
Gonzalez, F.J., Somoza, L., Hein, J.R., Medialdea, T., Leon, R., Urgorri, V., Reyes, J., Martin-Rubi, J.A., 2016. Phosphorites, Co-rich Mn nodules, and Fe-Mn crusts from Galicia Bank, NE Atlantic: reflections of Cenozoic tectonics and paleoceanography. Geochem. Geophys. Geosyst. 17, 346–374.
Gromet, L.P., Haskin, L.A., Korotev, R.L., Dymek, R.F., 1984. The "north American shale composite": its compilation, major and trace element characteristics. Geochim. Cosmochim. Acta 48, 2469–2482.
Halbach, P., Hebisch, U., Scherhag, C., 1981. Geochemical variations of ferromanganese nodules and crusts from different provinces of the Pacific Ocean and their genetic control. Chem. Geol. 34, 3–17.
Haley, B.A., Klinkhammer, G.P., McManus, J., 2004. Rare earth elements in pore waters of marine sediments. Geochim. Cosmochim. Acta 68, 1265–1279.
Hatch, G.P., 2012. Dynamics in the global market for rare earths. Elements 8, 341–346.
Hein, J.M., Koschinsky, A., 2013. Deep-ocean ferromanganese crusts and nodules. Geochemistry of Mineral Deposits 13, 273–291.
Hein, J.R., Yeh, H.-W., Gunn, S.H., Sliter, W.V., Benninger, L.M., Wang, C.-H., 1993. Two major Cenozoic episodes of phosphogenesis recorded in equatorial Pacific seamount deposits. Paleoceanography 8 (2), 293–311.
Hein, J.M., Mizell, K., Koschinsky, A., Conrad, T.A., 2013. Deep-ocean mineral deposits as a source of critical metals for high- and green-technology applications: comparison with land-based resources. Ore Geol. Rev. 51, 1–14.
Jankowski, J.A., Zielke, W., 2001. The mesoscale sediment transport due to technical activities in the deep sea. Deep-Sea Res. II 48, 3487–3521.
Kasten, S., Glasby, G.P., Schulz, H.D., Friedrich, G., Andreev, S.I., 1998. Rare earth elements in manganese nodules from the South Atlantic Ocean as indicators of oceanic bottom water flow. Mar. Geol. 146, 33–52.
Kato, Y., Fujinaga, K., Nakamura, K., Takaya, Y., Kitamura, K., Ohta, J., Toda, R., Nakashima, T., Iwamori, H., 2011. Deep-sea mud in the Pacific Ocean as a potential resource for rare-earth elements. Nat. Geosci. 4, 535–539.
Koschinsky, A., Hein, J.R., 2003. Uptake of elements from seawater by ferromanganese crusts: solid-phase associations and seawater speciation. Mar. Geol. 198 (3), 331–351.
Lee, J.H., Byrne, R.H., 1992. Examination of comparative rare earth element complexation behavior using linear free-energy relationships. Geochim. Cosmochim. Acta 56 (3), 1127–1137.
Li, Y.-H., 1981. Ultimate removal mechanisms of elements from the ocean. Geochim. Cosmochim. Acta 46, 1053–1060.
Lifton, J., 2009. The Lower Price Hybrid Fighter soon to Be Offered by Toyota. Has Toyota Discovered Rare Metal Auditing and Conservation? The Chinese society of rare earths
Luo, Y.R., Byrne, R.H., 2004. Carbonate complexation of yttrium and the rare earth elements in natural waters. Geochim. Cosmochim. Acta 68 (4), 691–699.
Mantyla, A.W., Reid, J.L., 1983. Abyssal characteristics of the world ocean waters. Deep Sea Research Part A 30, 805–833.
Miljutin, D.M., Miljutina, M.A., Arbizu, P.M., Galeron, J., 2011. Deep-sea nematode assemblage has not recovered 26 years after experimental mining of polymetallic nodules (clarion Clipperton fracture zone, tropical eastern Pacific). Deep Sea Research Part I 58 (8), 885–897.
Mills, R.A., Wells, D.M., Roberts, S., 2001. Genesis of ferromanganese crusts from the TAG hydrothermal field. Chem. Geol. 176 (1), 283–293.
Nagarajan, R., Madhavaraju, J., Armstrong-Altrin, J.S., Nagendra, R., 2011. Geochemistry of Neoproterozoic limestones of the Shahabad formation, Bhima Basin, Karnataka, southern India. Geosci. J. 15, 9–25.
Nath, B.N., Balaram, V., Sudhakar, M., Plüger, W.L., 1992. Rare earth element geochemistry of ferromanganese deposits from the Indian Ocean. Mar. Chem. 38, 185–208.
Orris, G.J., Grauch, R.I., 2002. Rare Earth Element Mines, Deposits and Occurrences (Vol. 2, No. 189). US Department of the Interior, US Geological Survey.
Pattan, J.N., Colley, S., Higgs, N.C., 1994. Behaviour of rare earth elements in coexisting manganese macronodules, micronodules, and sediments from the central Indian Basin. Mar. Georesour. Geotechnol. 12, 283–295.
Piper, D.Z., 1974. Rare earth elements in ferromanganese nodules and other marine phases. Geochim. Cosmochim. Acta 38, 1007–1022.
Rapin, F., Tessier, A., Campbell, P.G., Carignan, R., 1986. Potential artifacts in the determination of metal partitioning in sediments by a sequential extraction procedure. Environ. Sci. Technol. 20 (8), 836–840.
Reid, J.L., 1997. On the total geostrophic circulation of the Pacific Ocean: flow patterns, tracers, and transports. Prog. Oceanogr. 39, 263–352.
Schijf, J., Marshall, K.S., 2011. YREE sorption on hydrous ferric oxide in 0.5 M NaCl solutions: a model extension. Mar. Chem. 123, 32–43.
Sholkovitz, E.R., 1990. Rare-earth elements in marine sediments and geochemical standards. Chem. Geol. 88 (3–4), 333–347.
Sholkovitz, E.R., 1995. The aquatic chemistry of rare earth elements in rivers and estuaries. Aquat. Geochem. 1 (1), 1–34.
Sholkovitz, E.R., Landing, W.M., Lewis, B.L., 1994. Ocean particle chemistry: the fractionation of rare earth elements between suspended particles and seawater. Geochim. Cosmochim. Acta 58, 1567–1579.
Sval'nov, V.N., Lyapin, A.B., Novikova, Z.T., 1991. Manganese micronodules: communication 2. Composition and origin. Lithol. Miner. Resour. 26 (4), 32–50.
Sverdrup, H.U., Johnson, M.W., Fleming, R.H., 1970. The Oceans. Prentice Hall, Englewood Cliffs, N.J 1087 pp.
Thomson, J., Carpenter, M.S.N., Colley, S., Wilson, T.R.S., 1984. Metal accumulation rates in Northwest Atlantic pelagic sediments. Geochim. Cosmochim. Acta 48, 1935–1948.
Toyoda, K., Nakamura, Y., Masuda, A., 1990. Rare earth elements of Pacific pelagic sediments. Geochim. Cosmochim. Acta 54, 1093–1103.
Turekian, K., Imbrie, J., 1966. The distribution of trace elements in deep-sea sediments of the Atlantic Ocean. Earth Planet. Sci. Lett. 1, 161–168.
U.S. Geological Survey, 2014. Mineral Commodity Summaries February 2014.
Wegorzewski, A.V., Kuhn, T., 2014. The influence of suboxic diagenesis on the formation of manganese nodules in the clarion Clipperton nodule belt of the Pacific Ocean. Mar. Geol. 357, 123–138.
Winters, G.V., Buckley, D.E., 1992. Factor Analyses as a Method of Evaluation Sediment Environmental Quality in Halifax Harbour, Nova Scotia. Geological Survey of Canada, Current Research, Part D, Paper 92-1D. pp. 165–171.
Zhang, Z.G., Du, Y.S., Gao, L.F., Zhang, Y., Shi, G.Y., Liu, C.S., Zhang, P., Duan, X.K., 2012. Enrichment of REEs in polymetallic nodules and crusts and its potential for exploitation. J. Rare Earths 30, 621–626.
Zhong, S.J., Mucci, A., 1995. Partitioning of rare earth elements (REEs) between calcite and seawater solutions at 25 °C and 1 atm, and high dissolved REE concentrations. Geochim. Cosmochim. Acta 59 (3), 443–453.